

Generalist Equivariant Transformer Towards 3D Molecular Interaction Learning

Xiangzhe Kong^{1,2} Wenbing Huang³ Yang Liu^{1,2}

¹Dept. of Comp. Sci. & Tech., Institute for AI, BNRist Center, Tsinghua University

²Institute for AIR, Tsinghua University

³Gaoling School of Artificial Intelligence, Renmin University of China

jackie_kxz@outlook.com, hwenbing@126.com, liuyang2011@tsinghua.edu.cn

Abstract

Many processes in biology and drug discovery involve various 3D interactions between different molecules, such as protein and protein, protein and small molecule, etc. Designing a generalist model to learn universal molecular interactions is valuable yet challenging, given that different molecules are usually represented in different granularity. In this paper, we first propose to universally represent a 3D molecule as a geometric graph of sets, in contrast to conventional single-level representations. Upon the proposed unified representation, we then propose a Generalist Equivariant Transformer (GET) to effectively capture both sparse block-level and dense atom-level interactions. To be specific, GET consists of a bilevel attention module, a feed-forward module and a layer normalization module, where, notably, each module is $E(3)$ equivariant to meet the symmetry of 3D world. Extensive experiments on the prediction of protein-protein affinity, ligand binding affinity, and ligand efficacy prediction verify the effectiveness of our proposed method against existing methods, and reveal its potential to learn transferable knowledge across different domains and different tasks.

1 Introduction

Molecular interactions [47], which describe attractive or repulsive forces between molecules and between non-bonded atoms, are crucial in the research of chemistry, biochemistry and biophysics, and come as foundation processes of various downstream applications, including drug discovery, material design, etc [38, 49, 50]. There are different types of molecular interactions. In this paper, we mainly focus on the ones that exist in bimolecular complexes, such as protein and protein complexes, protein and small molecular complexes. Specifically, to better capture their physical effects, we study molecular interactions via 3D geometry where atom coordinates are always provided.

Modeling molecular interaction relies heavily on how to represent molecules appropriately. In recent studies, Graph Neural Networks (GNNs) are applied for this purpose [13, 22]. This is motivated by the fact that graphs naturally represent molecules, by considering atoms as nodes and inter-atom interactions or bonds as edges. When further encapsulating 3D atom coordinates, geometric graphs [11, 41, 44] are used in place of conventional notions that solely encode topology. To process geometric graphs, equivariant GNNs, a new kind of GNNs that meet $E(3)$ equivariance regarding translation, rotation and reflection are proposed, which exhibit promising performance in molecule interaction tasks [29, 31, 48, 58].

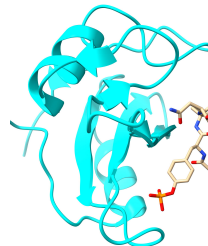


Figure 1: The interface of a protein interacting with a small molecule.

Despite the encouraging progress, there still lacks a desirable and unified form of cross-domain molecular representation in molecular interaction. The molecules of different domains like small molecules, proteins, and DNA are usually represented in different granularity, which consist of atoms, residues, and nucleobases, respectively. In the graph representation, their nodes correspond to building blocks of different granularity. Directly applying such unshared block-level representation leads to limited transferability of the models from one domain to another. One possible way to derive universal representation is to decompose all kinds of molecules into graphs of atoms, since any block itself is a set of atoms (*e.g.*, a residue consists of backbone and side-chain atoms). However, the atom-level representation discards the block specificity (*e.g.* which residue each atom belongs to) and will overlook valuable heuristics for representation learning. Therefore, it is valuable yet challenging to design a universal representation and a generalist model thereon, to capture both the block-level specificity and atom-level shareability.

In this paper, we propose a unified representation mechanism by modeling a complex involved in molecular interaction as a *geometric graph of sets*. This representation follows a bilevel design: in the top level, a complex is represented as a geometric graph of blocks; in the bottom level, each block contains a set of atomic instances. It is nontrivial to process such bilevel geometric graphs, as the model should handle blocks of variable sizes and ensure certain specific geometries. To this end, we propose *Generalist Equivariant Transformer (GET)*, which consists of the three modules: bilevel attention module, feed-forward module and layer normalization module. To be specific, the bilevel attention module updates the information of each atom by adopting both sparse block-level and dense atom-level attentions. By its design, this module is $E(3)$ -equivariant regarding the 3D coordinates and permutation-invariant regarding all atoms within each block, and works regardless of the block size. The feed-forward module is to inject the intra-block geometry to each atom, and the layer normalization module is proposed to stabilize and accelerate the training, both of which are designed to be $E(3)$ -equivariant.

We conduct experiments on three tasks concerning molecular interaction: protein-protein affinity (PPA), ligand binding affinity (LBA), and ligand efficacy prediction (LEP). The results exhibit the superiority of our GET on the proposed unified representation over traditional methods based on single-level representation. More excitingly, we identify strong potential of GET to capture and transfer universal knowledge across different tasks. We perform joint training of GET on both PPA and LBA, and observe that the performance is enhanced than its single-task counterparts particularly for PPA. The details are provided in our experiments.

2 Related Work

Molecular Interaction and Representation Various types of molecules across different domains [7, 8, 26] can form interactions, the strength of which are usually measured by the energy gap between the unbound and bound states of the molecules (*i.e.* affinity) [14]. Particularly, we focus on interactions between two proteins [26], as well as between a protein and a small molecule [7], both of which are widely explored in the machine learning community [28, 32, 31, 43, 44, 53]. Small molecules are usually represented by graphs where nodes are atoms [2, 18, 56, 57], but there are also explorations on subgraph-level decomposition of molecules by mining motifs [12, 22, 29]. Proteins are built upon residues, which are predefined sets of atoms [37], and thus have mainly two categories of representations according to the granularity of graph nodes: atom-level and residue-level. Atom-level representations, as the name suggests, decompose proteins into single atoms [48] and discard the hierarchy of proteins. Residue-level representations either exert pooling on the atoms [23], or directly use residue-specific features [1, 42, 43, 53] which is limited to proteins. Despite the differences in building blocks, the basic units (*i.e.* atoms) are shared across different types of molecules, and so do the fundamental regularities. Therefore, it is valuable to construct a unified representation of different type of molecules, which is explored in this paper.

Equivariant Network Equivariant networks integrate the symmetry of 3D world, namely $E(3)$ -equivariance, into the models, and thus are widely used in geometric learning [11, 40, 46]. Our work is inspired by multi-channel equivariant graph neural networks [19, 29] which assign each node with a coordinate matrix. However, they require a fixed number of channels (*i.e.* constant number of rows in the coordinate matrix) and lack invariance w.r.t to the permutations of the coordinates, which limits their application here as each building block is an unordered set of atoms with variable size.

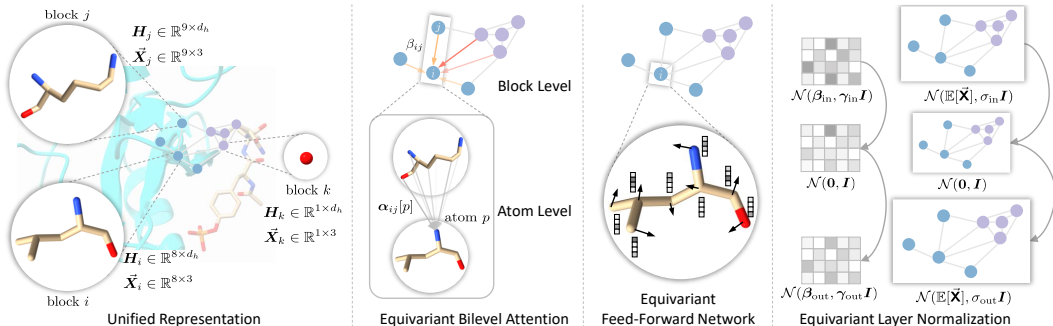


Figure 2: Overview of the unified representation and the equivariant modules in our Generalist Equivariant Transformer (GET). From left to right: The unified representation treats molecules as geometric graphs of sets according to predefined building blocks; The bilevel attention module captures both sparse block-level and dense atom-level interactions via an equivariant attention mechanism; The feed-forward network injects the block-level information into the intra-block atoms; The layer normalization transforms the input distribution with trainable scales and offsets.

Moreover, the node features are still limited to single vector form, which is unable to accommodate all-atom representations in single blocks. In contrast, our proposed model is designed to handle geometric graphs of sets where each node contains an unordered set of 3D instances with a different size, which fits perfectly with the concept of building blocks in molecules.

3 Method

We start by illustrating the proposed unified representation for proteins and small molecules in § 3.1. Then we introduce GET in § 3.2. Each layer of GET consists of the three types of E(3)-equivariant modules: a bilevel attention module, a feed-forward module, and a layer normalization after each previous module. The overall concepts are depicted in Figure 2.

3.1 Unified Representation: Geometric Graphs of Sets

Graphs come as a central tool for the representation of molecules, and different kind of graphs is applied in different case. For instance, small molecules can be represented as single-level graphs, where each node is an atom, while proteins correspond to two-level graphs, where each node is a residue that consists of a variable number of atoms. To better characterize the interaction between different molecules, below we propose a unified representation for proteins and small molecules.

Given a complex consisting of a set of atoms \mathbb{A} , we first identify a set of blocks (*i.e.* subgraphs) from \mathbb{A} according to some predefined notions (*e.g.* residues for proteins). Then the complex is abstracted as a geometric graph of sets $\mathcal{G} = (\mathcal{V}, \mathcal{E})$, where $\mathcal{V} = \{(\mathbf{H}_i, \vec{\mathbf{X}}_i) | 1 \leq i \leq B\}$ includes all B blocks and $\mathcal{E} = \{(i, j, \mathbf{e}_{ij}) | 1 \leq i, j \leq B\}$ includes all edges between blocks¹, where $\mathbf{e}_{ij} \in \mathbb{R}^{d_e}$ distinguishes the type of the edge as intra-molecular or inter-molecular connection. In each block composed of n_i atoms, $\mathbf{H}_i \in \mathbb{R}^{n_i \times d_h}$ denotes a set of atom feature vectors and $\vec{\mathbf{X}}_i \in \mathbb{R}^{n_i \times 3}$ denotes a set of 3D atom coordinates. To be specific, the p -th row of \mathbf{H}_i , which is the feature vector of atom p , sums up the trainable embeddings of atom types $\mathbf{a}_i[p]$, block types b_i , and atom position codes $\mathbf{p}_i[p]$ (see Appendix A), namely, $\mathbf{H}_i[p] = \text{Embed}(\mathbf{a}_i[p]) + \text{Embed}(b_i) + \text{Embed}(\mathbf{p}_i[p]) \in \mathbb{R}^{d_h}$, $1 \leq p \leq n_i$. To reduce the computational complexity, we construct \mathcal{E} via k-nearest neighbors according to the block distance which is defined as the minimum distance between inter-block atom pairs:

$$d(i, j) = \min\{\|\vec{\mathbf{X}}_i[p] - \vec{\mathbf{X}}_j[q]\|_2 \mid 1 \leq p \leq n_i, 1 \leq q \leq n_j\}. \quad (1)$$

As we will observe in the next section, the above bilevel design allows our model to capture sparse interactions for the top level and dense interactions for the bottom level, achieving a desirable integration of different granularities.

In this paper, we focus on proteins and small molecules, whose building blocks are conventionally defined as residues [59] and atoms [20, 57], respectively. Note that the representation can be easily extended to arbitrary block definitions (*e.g.* subgraph-level decomposition of small molecules [12,

¹We have added self-loops to reflect self-interactions between the atoms in each block.

29]), and therefore it can accommodate other types of molecules as well (e.g. DNA, with nucleobases as building blocks [3, 55]).

Connection to Single-Level Representations If we restrict the blocks to one-atom subsets only, then we obtain the **atom-level** representation where each node is one atom, and correspondingly both \mathbf{H}_i and $\vec{\mathbf{X}}_i$ are downgraded to row vectors as $n_i \equiv 1$. If we retain the building blocks but replace \mathbf{H}_i and $\vec{\mathbf{X}}_i$ with their centroids, then we obtain the **block-level** representation where the atoms in the same block are pooled into one single instance. Both single-level representations assign a vector and a 3D coordinate to each node, hence can be fed into most structural learning models [11, 40, 41, 46]. In contrast, the proposed bilevel representation requires the capability of processing E(3)-equivariant feature matrices (\mathbf{H}_i and $\vec{\mathbf{X}}_i$) with a variable number of rows, which cannot be directly processed by existing models. Additionally, within each block, the rows of \mathbf{H}_i and $\vec{\mathbf{X}}_i$ are indeed elements in a set and their update should be unaffected by the row order. Luckily, the above challenges are well handled by our Generalist Equivariant Transformer proposed in the next section.

3.2 Generalist Equivariant Transformer

Upon the unified representation, we propose GET to model the structure of the input complex. As mentioned above, one beneficial property of GET is that it can tackle blocks of variable size. Besides, GET is sophisticatedly designed to ensure E(3)-equivariance and intra-block permutation invariance to handle the symmetry. Specifically, each layer of GET first exploits an equivariant bilevel attention module to capture both sparse interactions in block level and dense interactions in atom level. Then an equivariant feed-forward module updates each atom with the representation and geometry of its block. Finally, a novel equivariant layer normalization is implemented on both the hidden states and coordinates. We present a detailed scheme of GET in Appendix B for better understanding.

Equivariant Bilevel Attention Module Given two blocks i and j of n_i and n_j atoms, respectively, we first obtain the query, the key, and the value matrices as follows:

$$\mathbf{Q}_i = \mathbf{H}_i \mathbf{W}_Q, \quad \mathbf{K}_j = \mathbf{H}_j \mathbf{W}_K, \quad \mathbf{V}_j = \mathbf{H}_j \mathbf{W}_V, \quad (2)$$

where $\mathbf{W}_Q, \mathbf{W}_K, \mathbf{W}_V \in \mathbb{R}^{d_h \times d_r}$ are trainable parameters. We denote $\vec{\mathbf{X}}_{ij} \in \mathbb{R}^{n_i \times n_j \times 3}$ and $\mathbf{D}_{ij} \in \mathbb{R}^{n_i \times n_j}$ as the relative coordinates and distances between any atom pair in block i and j , namely, $\vec{\mathbf{X}}_{ij}[p, q] = \vec{\mathbf{X}}_i[p] - \vec{\mathbf{X}}_j[q]$, $\mathbf{D}_{ij}[p, q] = \|\vec{\mathbf{X}}_{ij}[p, q]\|_2$.

The **atom-level cross attention values** from j to i are calculated by:

$$\mathbf{R}_{ij} = \frac{1}{\sqrt{d_r}} (\mathbf{Q}_i \mathbf{K}_j^\top) + \sigma_D(\mathbf{D}_{ij}), \quad (3)$$

$$\alpha_{ij} = \text{Softmax}(\mathbf{R}_{ij}). \quad (4)$$

Here, σ_D is an element-wise activation function implemented by a Multi-Layer Perceptron (MLP). $\mathbf{R}_{ij} \in \mathbb{R}^{n_i \times n_j}$ represents the correlation between each atom in block i and j , and it is computed by a normalized inner-product term $\mathbf{Q}_i \mathbf{K}_j^\top$ plus distance activation $\sigma_D(\mathbf{D}_{ij})$. The elements of $\alpha_{ij} \in \mathbb{R}^{n_i \times n_j}$ are the atom-level cross attentions between the two blocks.

The **block-level cross attention value** from j to i is given by:

$$r_{ij} = \frac{\mathbf{1}^\top \mathbf{R}_{ij} \mathbf{1}}{n_i n_j} + \phi_e(e_{ij}), \quad (5)$$

$$\beta_{ij} = \frac{\exp(r_{ij})}{\sum_{j \in \mathcal{N}(i)} \exp(r_{ij})}, \quad (6)$$

where $\mathbf{1}$ is the column vector whose elements are all ones, e is the optional edge feature which we use to distinguish between intra-molecule edges and inter-molecule edges, ϕ_e is an MLP projecting the edge feature to a scalar, and $\mathcal{N}(i)$ denotes the neighborhood blocks of i . Basically, r_{ij} represents the global correlation between i and j after aggregating all values in \mathbf{R}_{ij} and edge e_{ij} . Then, β_{ij} represents the block-level cross attention.

With the atom-level and the block-level attentions at hand, we are ready to update both the hidden states and coordinates for each atom p in block i :

$$\mathbf{H}'_i[p] = \mathbf{H}_i[p] + \sum_{j \in \mathcal{N}(i)} \beta_{ij} \phi_m(\alpha_{ij}[p] \cdot \mathbf{V}_j), \quad (7)$$

$$\vec{\mathbf{X}}'_i[p] = \vec{\mathbf{X}}_i[p] + \sum_{j \in \mathcal{N}(i)} \beta_{ij} (\alpha_{ij}[p] \odot \phi_X(\mathbf{R}_{ij}[p])) \cdot \vec{\mathbf{X}}_{ij}[p], \quad (8)$$

where, ϕ_m is an MLP, ϕ_X is an element-wise MLP to process the input vector, and \odot computes the element-wise multiplication. It is verified that the shape of the updated variables \mathbf{H}'_i and $\vec{\mathbf{X}}'_i$ keeps the same regardless of value of the block size n_j . In addition, since the attentions α_{ij} and β_{ij} are E(3)-invariant, the update of $\vec{\mathbf{X}}'_i$ is E(3)-equivariant. It can also be observed that the update is independent to the atom permutation of each block. We provide detailed proofs in Appendix C.

Equivariant Feed-Forward Network This module updates \mathbf{H}_i and $\vec{\mathbf{X}}_i$ for each atom individually. We denote each row of \mathbf{H}_i as \mathbf{h} , and $\vec{\mathbf{X}}_i$ as $\vec{\mathbf{x}}$. We first calculate the centroids of the block:

$$\mathbf{h}_c = \text{centroid}(\mathbf{H}_i), \quad \vec{\mathbf{x}}_c = \text{centroid}(\vec{\mathbf{X}}_i). \quad (9)$$

Then we obtain the relative coordinate $\Delta\vec{\mathbf{x}}$ as well as the distance representation (\mathbf{r}) between each atom and the centroid:

$$\Delta\vec{\mathbf{x}} = \vec{\mathbf{x}} - \vec{\mathbf{x}}_c, \quad \mathbf{r} = \phi_r\left(\frac{\Delta\vec{\mathbf{x}}^\top \Delta\vec{\mathbf{x}}}{C + \|\Delta\vec{\mathbf{x}}^\top \Delta\vec{\mathbf{x}}\|}\right), \quad (10)$$

where $C = 1$ is a constant and used to avoid exploding numerical values [39]. The centroids and the distance representation are then integrated into the updating process of \mathbf{h} and $\vec{\mathbf{x}}$ to let each atom be aware of the geometric context of its block, where ϕ_x is an MLP that returns a scalar:

$$\mathbf{h}' = \mathbf{h} + \phi_h(\mathbf{h}, \mathbf{h}_c, \mathbf{r}), \quad (11)$$

$$\vec{\mathbf{x}}' = \vec{\mathbf{x}} + \Delta\vec{\mathbf{x}} \phi_x(\mathbf{h}, \mathbf{h}_c, \mathbf{r}), \quad (12)$$

Equivariant Layer Normalization Layer normalization is known to stabilize and accelerate the training of deep neural networks [4] and is also an essential component in the well-known Transformer [51]. The challenge here is that we need to additionally consider the symmetry of the 3D world (i.e. E(3)-equivariance) when normalizing the coordinates. To this end, we first extract the centroid of the entire graph as $\mathbb{E}[\vec{\mathbf{X}}]$, where $\vec{\mathbf{X}}$ collects the coordinates of all atoms in all blocks. Then we exert layer normalization on the hidden vectors and coordinates of individual atoms as follows:

$$\mathbf{h} = \frac{\mathbf{h} - \mathbb{E}[\mathbf{h}]}{\sqrt{\text{Var}[\mathbf{h}]}} \cdot \gamma + \beta, \quad (13)$$

$$\vec{\mathbf{x}} = \frac{\vec{\mathbf{x}} - \mathbb{E}[\vec{\mathbf{X}}]}{\sqrt{\text{Var}[\vec{\mathbf{X}} - \mathbb{E}[\vec{\mathbf{X}}]]}} \cdot \sigma + \mathbb{E}[\vec{\mathbf{X}}], \quad (14)$$

where γ, β , and σ are learnable parameters, and $\text{Var}[\vec{\mathbf{X}} - \mathbb{E}[\vec{\mathbf{X}}]]$ calculates the variation of all atom coordinates with respect to the centroid. Therefore, the coordinates, after subtracting the centroid of all atoms, are first normalized to standard Gaussian distribution and then scaled with σ before recovering the centroid.

Thanks to the E(3)-equivariance of each module, GET, which is the cascading of these modules in each layer, also conforms to the symmetry of the 3D world. We provide the proof in Appendix C.

4 Experiments

We conduct experiments on three challenging tasks concerning molecular interactions to validate the efficacy of the unified representation as well as the proposed GET: protein-protein affinity (PPA, § 4.1), ligand binding affinity (LBA, § 4.2), and ligand efficacy prediction (LEP, § 4.3). We further explore the ability of our method to capture the universal and transferable atomic interaction mechanism in § 4.4 by training the model on the mixed dataset of PPA and LBA, then conduct evaluation on the test sets of PPA and LBA separately. Molecular interactions mainly require analysis in the scope of the interface [7, 33, 34], thus the input graphs contain blocks of each molecule within 6Å distance to its interacting partner [48]. Implementation details are provided in Appendix D.

Baselines Four baselines are shared across different tasks. **SchNet** [41] implements continuous-filter convolution on the 3D molecular graph to capture the geometry. **DimeNet++** [11, 10] exploits the radial basis function (RBF) and the spherical basis function (SBF) as input features to learn both the spatial distance and directions with directional message passing. **EGNN** [40] is a lightweight yet effective E(n)-equivariant graph neural network using only relative distances for geometric learning. **TorchMD-Net** [46] utilizes RBF to define the geometry and proposes an equivariant attention mechanism to compose an equivariant graph Transformer. We assess each baseline with two single-level representations mentioned in § 3.1, namely the block-level and the atom-level representations. Please refer to Appendix E for implementation details. For LBA and LEP, which come from the Atom3D benchmark [48], we also include the results of existing benchmarked atom-level baselines: **Atom3D-CNN** [48], **Atom3D-ENN** [48], **Atom3D-GNN** [48], as well as **GVP-GNN** [24].

4.1 Protein-Protein Affinity

This task aims to predict the affinity of two proteins given the binding complex. To this end, we implement sum pooling on the atom-wise representations given by our GET in each block, then normalize the obtained vectors as block-level representations. The same procedure are repeated on the block level to obtain the graph-level representation, which is then projected to the value of affinity by an MLP head. For quantitative evaluation, we adopt the following two widely used metrics [30, 32, 35]: **Pearson Correlation** [6] measures the linear correlation between the predicted values and the target values; **Spearman Correlation** [16] measures the correlation between the rankings given by the predicted and the target values.

Table 1: The mean and the standard deviation of three runs on protein-protein affinity prediction. The best results are marked in bold and the second best are underlined.

Repr.	Model	Rigid	Medium	Flexible	All
Pearson↑					
Block	SchNet	0.542 ± 0.012	0.504 ± 0.020	0.102 ± 0.019	<u>0.439 ± 0.016</u>
	DimeNet++	0.487 ± 0.087	0.367 ± 0.043	<u>0.152 ± 0.078</u>	0.323 ± 0.025
	EGNN	0.437 ± 0.023	0.436 ± 0.028	0.094 ± 0.049	0.381 ± 0.021
	TorchMD-Net	0.575 ± 0.041	0.470 ± 0.024	0.087 ± 0.024	0.424 ± 0.021
Atom	SchNet	0.592 ± 0.007	<u>0.522 ± 0.010</u>	-0.038 ± 0.016	0.369 ± 0.007
	DimeNet++ ²	-	-	-	-
	EGNN	0.497 ± 0.027	0.452 ± 0.012	-0.054 ± 0.013	0.302 ± 0.010
	TorchMD-Net	0.609 ± 0.023	0.486 ± 0.004	0.049 ± 0.009	0.401 ± 0.005
Unified	GET (ours)	<u>0.604 ± 0.016</u>	0.524 ± 0.013	0.301 ± 0.056	0.481 ± 0.008
Spearman↑					
Block	SchNet	0.476 ± 0.015	0.520 ± 0.013	0.068 ± 0.009	0.427 ± 0.012
	DimeNet++	0.466 ± 0.088	0.368 ± 0.037	0.171 ± 0.054	0.317 ± 0.031
	EGNN	0.364 ± 0.043	0.455 ± 0.026	0.080 ± 0.038	0.382 ± 0.022
	TorchMD-Net	0.552 ± 0.039	0.482 ± 0.025	0.090 ± 0.062	0.415 ± 0.027
Atom	SchNet	0.546 ± 0.005	0.512 ± 0.007	0.028 ± 0.032	0.404 ± 0.016
	DimeNet++	-	-	-	-
	EGNN	0.450 ± 0.042	0.438 ± 0.021	0.027 ± 0.030	0.349 ± 0.009
	TorchMD-Net	0.582 ± 0.025	0.487 ± 0.002	0.117 ± 0.008	<u>0.436 ± 0.004</u>
Unified	GET (ours)	<u>0.580 ± 0.011</u>	0.527 ± 0.005	0.300 ± 0.056	0.495 ± 0.011

Dataset We adopt the Protein-Protein Affinity Benchmark Version 2 [27, 52] as the test set, which contains 176 diversified protein-protein complexes with annotated affinity collected from existing literature. These complexes are further categorized into three difficulty levels (i.e. Rigid, Medium, Flexible) according to the conformation change of the proteins from the unbound to the bound state [27], among which the Flexible split is the most challenging as the proteins undergo large conformation change upon binding. As for training, we first filter out 2,500 complexes with annotated binding affinity (K_i or K_d) from PDBbind [54]. Then we use MMseqs2 [45] to cluster the sequences of these complexes together with the test set by dividing complexes with sequence identity above 30% into the same cluster, where sequence identity is calculated based on the BLOSUM62 substitution

²We failed to run atom-level DimeNet++ due to the high complexity of the angular SBF.

matrix [17]. The complexes that shares the same clusters with the test set are dropped to prevent data leakage, after which we finally obtained 2,195 valid complexes. We split these complexes into training set and validation set with a ratio of 9:1 with respect to the number of clusters. Following previous literature [5, 21, 36], we predict the negative log-transformed value (pK) instead of direct regression on the affinity.

Results We run three parallel experiments with different random seed for splitting the dataset and training the models. We report the mean and the standard deviation of Pearson Correlation and Spearman Correlation on different difficulty levels as well as on the overall test set in Table 1. It is observed that our GET with the unified representation generally achieves better performance than the baselines with either block-level representation or atom-level representation, which reveals the superiority of the unified bilevel representation over the single-level representations. An interesting observation is that block-level baselines tend to perform worse than their atom-level counterparts on easier splits, while the opposite is true on the harder splits. This is because higher difficulty indicates higher contribution of the conformation change to the affinity, thus demands more attention on the global geometry exhibiting in block level in addition to the fine-grained atom-level geometry. In this sense, GET captures more general interaction mechanism by modeling the sparse block-level interactions and the dense atom-level interactions simultaneously, and thus exhibits more gains over the baselines as the difficulty level increases. Notably, GET surpasses the baselines by a large margin on the hardest split (i.e. Flexible) on which the baselines display very weak correlation.

4.2 Ligand Binding Affinity

This task predicts the affinity of receptor-ligand complexes where the receptor is a protein and the ligand is a small molecule. We use the same strategy to formalize the task as a graph-level regression problem as in § 4.1. As for evaluation, in addition to **Pearson Correlation** and **Spearman Correlation**, we also report the Root Mean Square Error (**RMSE**) the of predicted value, as suggested by Townshend et al. [48].

Dataset We use the LBA dataset and its splits in Atom3D benchmark [48], where there are 3507, 466, and 490 complexes in the training, the validation, and the test sets. The criterion of the splits is also based on the clustering results, where in each cluster the sequence identity of the receptors is above 30% [48]. The affinity value is in the negative log-transformed form as in § 4.1.

Table 2: The mean and the standard deviation of three runs on ligand binding affinity prediction and ligand efficacy prediction. The best results are marked in bold and the second best are underlined.

Repr.	Model	LBA			LEP	
		RMSE↓	Pearson↑	Spearman↑	AUROC↑	AUPRC↑
Block	SchNet	1.406 ± 0.020	0.565 ± 0.006	0.549 ± 0.007	0.732 ± 0.022	0.718 ± 0.031
	DimeNet++	1.391 ± 0.020	0.576 ± 0.016	0.569 ± 0.016	0.669 ± 0.014	0.609 ± 0.036
	EGNN	1.409 ± 0.015	0.566 ± 0.010	0.548 ± 0.012	<u>0.746 ± 0.017</u>	<u>0.755 ± 0.031</u>
	TorchMD-net	1.367 ± 0.037	<u>0.599 ± 0.017</u>	0.584 ± 0.025	0.744 ± 0.034	0.721 ± 0.052
Atom	Atom3D-CNN	1.416 ± 0.021	0.550 ± 0.021	0.532 ± 0.032	0.589 ± 0.020	0.483 ± 0.037
	Atom3D-ENN	1.568 ± 0.012	0.389 ± 0.024	0.408 ± 0.021	0.663 ± 0.100	0.551 ± 0.121
	Atom3D-GNN	1.601 ± 0.048	0.545 ± 0.027	0.533 ± 0.033	0.681 ± 0.062	0.598 ± 0.135
	GVP-GNN	1.594 ± 0.073	-	-	0.628 ± 0.055	-
	SchNet	1.357 ± 0.017	0.598 ± 0.011	<u>0.592 ± 0.015</u>	0.712 ± 0.026	0.639 ± 0.033
	DimeNet++	1.439 ± 0.036	0.547 ± 0.015	0.536 ± 0.016	0.589 ± 0.049	0.503 ± 0.020
	EGNN	<u>1.358 ± 0.000</u>	<u>0.599 ± 0.002</u>	0.587 ± 0.004	0.711 ± 0.020	0.643 ± 0.041
	TorchMD-net	1.381 ± 0.013	0.591 ± 0.007	0.583 ± 0.009	0.677 ± 0.004	0.636 ± 0.054
Unified	GET (ours)	1.446 ± 0.012	0.600 ± 0.002	0.606 ± 0.002	0.757 ± 0.002	0.767 ± 0.010

Results We run three parallel experiments and report the mean and the standard deviation of the metrics in Table 2. The results of Atom3D baselines and GVP-GNN are copied from Townshend et al. [48] and Jing et al. [24], respectively. It reads that our model produces better or comparable performance compared to the baselines. The improvement is relatively minor compared to the PPA task in § 4.1, which is reasonable because the conventional building blocks of small molecules are single atoms and thus the unified representation of the ligand is downgraded to the atom-level representation. In addition, the benefit of capturing the top-level geometry in the receptor (i.e. protein)

is limited by the rigidity of interactions between proteins and small molecules [25, 15], where there is usually little conformation change upon binding [7]. Nevertheless, the unified representation still enhances the performance to some extent. We will further see the strength of the unified representation in the next task where interactions are also between proteins and small molecules but the top-level geometry really matters.

4.3 Ligand Efficacy Prediction

This task requires identifying a given ligand as the "activator" or the "inactivator" of a functional protein. Specifically, given the two complexes where the ligand interacts with the active and the inactive conformation of the protein respectively, the models need to distinguish which one is more favorable. To this end, we first obtain the graph-level representations of the two complexes as in § 4.1. Then we concatenate the two representations to do a binary classification. We use two metrics for evaluation: the area under the receiver operating characteristic (**AUROC**) and the area under precision-recall curve (**AUPRC**).

Dataset We follow the LEP dataset and its splits in the Atom3D benchmark [48], which includes 27 functional proteins and 527 ligands known as activator or inactivator to a certain protein. The active and the inactive complexes are generated by Glide [9]. The splits of the training, the validation, and the test sets are based on the functional proteins to ensure generalizability.

Results We present the mean and the standard deviation of the metrics across three runs in Table 2. Unlike LBA, LEP requires distinguishing the active and inactive conformations of the receptor, thus it is essential to capture the block-level geometry of the protein in addition to the atom-level receptor-ligand interactions. The unified representation excels at learning the bilevel geometry, therefore, naturally, we observe obvious gains on the metrics of our method compared to the baselines.

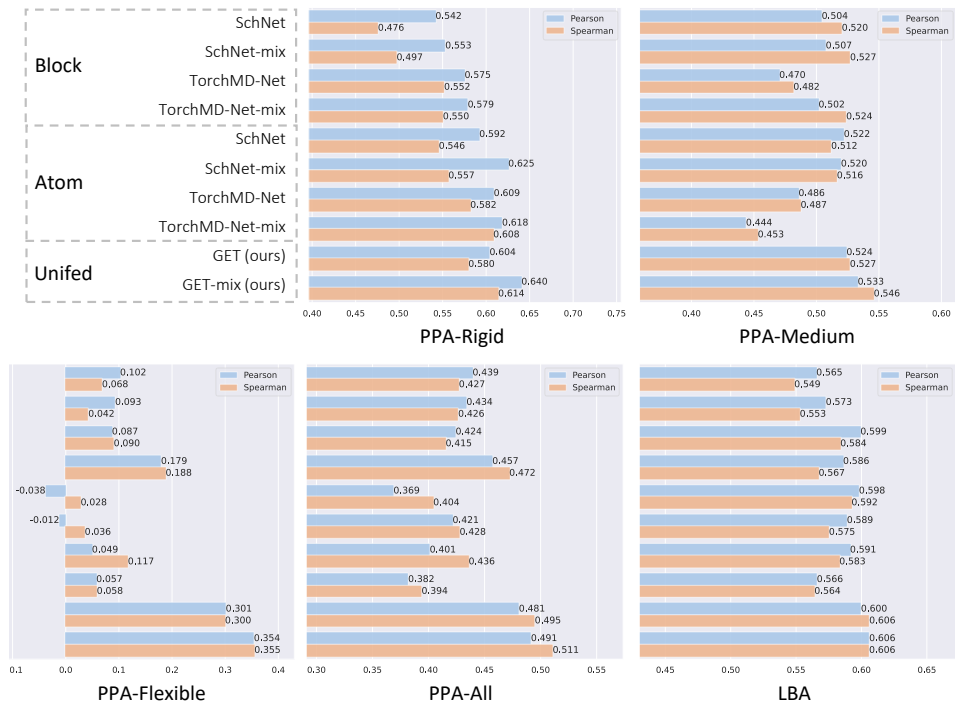


Figure 3: Comparison of different models on the universal learning of molecular interaction affinity. Methods with the suffix "-mix" are trained on the mixed dataset of PPA and LBA.

4.4 Universal Learning of Molecular Interaction Affinity

Finally, we explore whether our model is able to find universal underlying regularities that are transferable across different tasks and molecular types. To do this, we mix the dataset of PPA and

LBA for training, and evaluate the models on the test set of the two tasks, respectively. We also benchmark Schnet and TorchMD-Net, two strong baselines as shown in § 4.1 and § 4.2, under the same setting for comparison. We present the results in Figure 3, and include detailed mean and standard deviation in Appendix F. The results demonstrate that our method obtains great benefits from the mixed training set, especially on the PPA task, while the baselines receive minor improvement or even negative impact. These phenomena well demonstrate the generalization ability of the proposed Generalist Equivariant Transformer equipped with the unified representation.

5 Analysis

We first compare our GET with unified, block-level and atom-level representations, then we conduct ablation study by removing the following modules: the layer normalization (w/o LN); the equivariant normalization on coordinates in the LN (w/o equivLN); the equivariant feed-forward network (w/o FFN); both LN and FFN (w/o LN & FFN). The results are presented in Table 3.

We observe that GET with unified representation consistently surpasses GET with single-level representations, which again confirms the superiority of the unified bilevel representation, especially for tasks concerning molecules with well-defined hierarchies. The ablations of the modules reveal following regularities: (1) Removing either the entire layer normalization or only the equivariant normalization on coordinates introduces instability in training, which not only leads to higher variance across different experiments, but also induces adverse impacts in some tasks like PPA; (2) The removal of the equivariant feed-forward module incurs detriment to the overall performance, indicating the necessity of the FFN to encourage intra-block geometrical communications between atoms.

Table 3: Ablation study of each module in our proposed Generalist Equivariant Transformer (GET), where LN and FFN are abbreviations for LayerNorm and Feed-Forward Network, respectively. The best results are marked in bold and the second best are underlined.

Repr.	Model	PPA-All		LBA		LEP	
		Pearson \uparrow	Spearman \uparrow	Pearson \uparrow	Spearman \uparrow	AUROC \uparrow	AUPRC \uparrow
Unified	GET-mix	0.491 \pm 0.015	0.511 \pm 0.016	0.606 \pm 0.003	0.606 \pm 0.003	-	-
	GET	<u>0.481 \pm 0.008</u>	<u>0.495 \pm 0.011</u>	<u>0.600 \pm 0.002</u>	0.606 \pm 0.002	<u>0.757 \pm 0.002</u>	<u>0.767 \pm 0.010</u>
	w/o LN	0.401 \pm 0.038	0.384 \pm 0.051	0.596 \pm 0.003	0.602 \pm 0.005	0.760 \pm 0.003	0.770 \pm 0.008
	w/o equivLN	0.428 \pm 0.018	0.426 \pm 0.038	0.595 \pm 0.004	0.604 \pm 0.004	0.752 \pm 0.007	0.762 \pm 0.011
	w/o FFN	0.426 \pm 0.001	0.433 \pm 0.020	0.593 \pm 0.008	0.601 \pm 0.012	0.711 \pm 0.021	0.702 \pm 0.032
	w/o LN & FFN	0.456 \pm 0.055	0.470 \pm 0.073	0.588 \pm 0.003	0.594 \pm 0.007	0.713 \pm 0.018	0.720 \pm 0.035
Block	GET	0.444 \pm 0.018	0.448 \pm 0.034	0.595 \pm 0.008	<u>0.605 \pm 0.008</u>	0.755 \pm 0.006	0.765 \pm 0.008
Atom	GET	0.394 \pm 0.011	0.438 \pm 0.011	0.593 \pm 0.001	0.597 \pm 0.003	0.716 \pm 0.031	0.609 \pm 0.077

6 Limitations

Technically, our method can be extended to arbitrary definition of building blocks and thus can also generalize to other types of molecules as suggested in § 3.1, but we leave empirical evaluations for future work due to the absence of well-established benchmarks of other molecular types. Further, it is also possible to transfer atom-level knowledge across different molecular types in other scenarios apart from molecular interactions. For instance, universal pretraining on different kinds of molecules, which needs careful design of the unsupervised task, hence we also leave this for future work.

7 Conclusion

In this paper, we explore the unified representation of molecules as geometric graphs of sets, which enables all-atom representations while preserving the heuristic building blocks of different molecules. To model the unified representation, we propose a Generalist Equivariant Transformer (GET) to accommodate matrix-form node features and coordinates with E(3)-equivariance and permutation invariance. Each layer of GET consists of a bilevel attention module, a feed-forward module, and an equivariant layer normalization after each of the previous two modules. Experiments on molecular interactions demonstrate the superiority of learning unified representation with our GET compared to single-level representations and existing baselines. Further explorations on mixing molecular types reveal the ability of our method to learn generalizable molecular interaction mechanisms, which could inspire future research on universal representation learning of molecules.

References

- [1] N. Anand and T. Achim. Protein structure and sequence generation with equivariant denoising diffusion probabilistic models. *arXiv preprint arXiv:2205.15019*, 2022.
- [2] K. Atz, F. Grisoni, and G. Schneider. Geometric deep learning on molecular representations. *Nature Machine Intelligence*, 3(12):1023–1032, 2021.
- [3] Ž. Avsec, V. Agarwal, D. Visentin, J. R. Ledsam, A. Grabska-Barwinska, K. R. Taylor, Y. Assael, J. Jumper, P. Kohli, and D. R. Kelley. Effective gene expression prediction from sequence by integrating long-range interactions. *Nature methods*, 18(10):1196–1203, 2021.
- [4] J. L. Ba, J. R. Kiros, and G. E. Hinton. Layer normalization. *arXiv preprint arXiv:1607.06450*, 2016.
- [5] P. J. Ballester and J. B. Mitchell. A machine learning approach to predicting protein–ligand binding affinity with applications to molecular docking. *Bioinformatics*, 26(9):1169–1175, 2010.
- [6] I. Cohen, Y. Huang, J. Chen, J. Benesty, J. Benesty, J. Chen, Y. Huang, and I. Cohen. Pearson correlation coefficient. *Noise reduction in speech processing*, pages 1–4, 2009.
- [7] X. Du, Y. Li, Y.-L. Xia, S.-M. Ai, J. Liang, P. Sang, X.-L. Ji, and S.-Q. Liu. Insights into protein–ligand interactions: mechanisms, models, and methods. *International journal of molecular sciences*, 17(2):144, 2016.
- [8] A. A. Elfiky. Anti-hcv, nucleotide inhibitors, repurposing against covid-19. *Life sciences*, 248: 117477, 2020.
- [9] R. A. Friesner, J. L. Banks, R. B. Murphy, T. A. Halgren, J. J. Klicic, D. T. Mainz, M. P. Repasky, E. H. Knoll, M. Shelley, J. K. Perry, et al. Glide: a new approach for rapid, accurate docking and scoring. 1. method and assessment of docking accuracy. *Journal of medicinal chemistry*, 47(7):1739–1749, 2004.
- [10] J. Gasteiger, S. Giri, J. T. Margraf, and S. Günnemann. Fast and uncertainty-aware directional message passing for non-equilibrium molecules. *arXiv preprint arXiv:2011.14115*, 2020.
- [11] J. Gasteiger, J. Groß, and S. Günnemann. Directional message passing for molecular graphs. *arXiv preprint arXiv:2003.03123*, 2020.
- [12] Z. Geng, S. Xie, Y. Xia, L. Wu, T. Qin, J. Wang, Y. Zhang, F. Wu, and T.-Y. Liu. De novo molecular generation via connection-aware motif mining. *arXiv preprint arXiv:2302.01129*, 2023.
- [13] J. Gilmer, S. S. Schoenholz, P. F. Riley, O. Vinyals, and G. E. Dahl. Neural message passing for quantum chemistry. In *International conference on machine learning*, pages 1263–1272. PMLR, 2017.
- [14] M. K. Gilson, J. A. Given, B. L. Bush, and J. A. McCammon. The statistical-thermodynamic basis for computation of binding affinities: a critical review. *Biophysical journal*, 72(3): 1047–1069, 1997.
- [15] E. V. Gurevich and V. V. Gurevich. Therapeutic potential of small molecules and engineered proteins. *Arrestins-Pharmacology and Therapeutic Potential*, pages 1–12, 2014.
- [16] J. Hauke and T. Kossowski. Comparison of values of pearson’s and spearman’s correlation coefficients on the same sets of data. *Quaestiones geographicae*, 30(2):87–93, 2011.
- [17] S. Henikoff and J. G. Henikoff. Amino acid substitution matrices from protein blocks. *Proceedings of the National Academy of Sciences*, 89(22):10915–10919, 1992.
- [18] E. Hoogeboom, V. G. Satorras, C. Vignac, and M. Welling. Equivariant diffusion for molecule generation in 3d. In *International Conference on Machine Learning*, pages 8867–8887. PMLR, 2022.

- [19] W. Huang, J. Han, Y. Rong, T. Xu, F. Sun, and J. Huang. Equivariant graph mechanics networks with constraints. *arXiv preprint arXiv:2203.06442*, 2022.
- [20] R. Jiao, J. Han, W. Huang, Y. Rong, and Y. Liu. Energy-motivated equivariant pretraining for 3d molecular graphs. *arXiv preprint arXiv:2207.08824*, 2022.
- [21] J. Jiménez, M. Skalic, G. Martinez-Rosell, and G. De Fabritiis. K deep: protein–ligand absolute binding affinity prediction via 3d-convolutional neural networks. *Journal of chemical information and modeling*, 58(2):287–296, 2018.
- [22] W. Jin, R. Barzilay, and T. Jaakkola. Junction tree variational autoencoder for molecular graph generation. In *International conference on machine learning*, pages 2323–2332. PMLR, 2018.
- [23] W. Jin, R. Barzilay, and T. Jaakkola. Antibody-antigen docking and design via hierarchical equivariant refinement. *arXiv preprint arXiv:2207.06616*, 2022.
- [24] B. Jing, S. Eismann, P. N. Soni, and R. O. Dror. Equivariant graph neural networks for 3d macromolecular structure. *arXiv preprint arXiv:2106.03843*, 2021.
- [25] S. Jones and J. M. Thornton. Protein-protein interactions: a review of protein dimer structures. *Progress in biophysics and molecular biology*, 63(1):31–65, 1995.
- [26] S. Jones and J. M. Thornton. Principles of protein-protein interactions. *Proceedings of the National Academy of Sciences*, 93(1):13–20, 1996.
- [27] P. L. Kastiris, I. H. Moal, H. Hwang, Z. Weng, P. A. Bates, A. M. Bonvin, and J. Janin. A structure-based benchmark for protein–protein binding affinity. *Protein Science*, 20(3):482–491, 2011.
- [28] X. Kong, W. Huang, and Y. Liu. Conditional antibody design as 3d equivariant graph translation. *arXiv preprint arXiv:2208.06073*, 2022.
- [29] X. Kong, W. Huang, Z. Tan, and Y. Liu. Molecule generation by principal subgraph mining and assembling. *Advances in Neural Information Processing Systems*, 35:2550–2563, 2022.
- [30] X. Liu, Y. Luo, P. Li, S. Song, and J. Peng. Deep geometric representations for modeling effects of mutations on protein-protein binding affinity. *PLoS computational biology*, 17(8):e1009284, 2021.
- [31] S. Luo, Y. Su, X. Peng, S. Wang, J. Peng, and J. Ma. Antigen-specific antibody design and optimization with diffusion-based generative models. *bioRxiv*, pages 2022–07, 2022.
- [32] S. Luo, Y. Su, Z. Wu, C. Su, J. Peng, and J. Ma. Rotamer density estimator is an unsupervised learner of the effect of mutations on protein-protein interaction. *bioRxiv*, pages 2023–02, 2023.
- [33] R. M. MacCallum, A. C. Martin, and J. M. Thornton. Antibody-antigen interactions: contact analysis and binding site topography. *Journal of molecular biology*, 262(5):732–745, 1996.
- [34] I. M. Nooren and J. M. Thornton. Diversity of protein–protein interactions. *The EMBO journal*, 22(14):3486–3492, 2003.
- [35] P. Notin, M. Dias, J. Frazer, J. M. Hurtado, A. N. Gomez, D. Marks, and Y. Gal. Tranception: protein fitness prediction with autoregressive transformers and inference-time retrieval. In *International Conference on Machine Learning*, pages 16990–17017. PMLR, 2022.
- [36] M. Ragoza, J. Hochuli, E. Idrobo, J. Sunseri, and D. R. Koes. Protein–ligand scoring with convolutional neural networks. *Journal of chemical information and modeling*, 57(4):942–957, 2017.
- [37] J. S. Richardson. The anatomy and taxonomy of protein structure. *Advances in protein chemistry*, 34:167–339, 1981.
- [38] N. Sapoval, A. Aghazadeh, M. G. Nute, D. A. Antunes, A. Balaji, R. Baraniuk, C. Barberan, R. Dannenfels, C. Dun, M. Edrisi, et al. Current progress and open challenges for applying deep learning across the biosciences. *Nature Communications*, 13(1):1728, 2022.

- [39] V. G. Satorras, E. Hoogeboom, F. B. Fuchs, I. Posner, and M. Welling. E (n) equivariant normalizing flows. *arXiv preprint arXiv:2105.09016*, 2021.
- [40] V. G. Satorras, E. Hoogeboom, and M. Welling. E (n) equivariant graph neural networks. In *International conference on machine learning*, pages 9323–9332. PMLR, 2021.
- [41] K. Schütt, P.-J. Kindermans, H. E. Sauceda Felix, S. Chmiela, A. Tkatchenko, and K.-R. Müller. Schnet: A continuous-filter convolutional neural network for modeling quantum interactions. *Advances in neural information processing systems*, 30, 2017.
- [42] C. Shi, C. Wang, J. Lu, B. Zhong, and J. Tang. Protein sequence and structure co-design with equivariant translation. *arXiv preprint arXiv:2210.08761*, 2022.
- [43] V. R. Somnath, C. Bunne, and A. Krause. Multi-scale representation learning on proteins. *Advances in Neural Information Processing Systems*, 34:25244–25255, 2021.
- [44] H. Stärk, D. Beaini, G. Corso, P. Tossou, C. Dallago, S. Günnemann, and P. Liò. 3d infomax improves gnns for molecular property prediction. In *International Conference on Machine Learning*, pages 20479–20502. PMLR, 2022.
- [45] M. Steinegger and J. Söding. Mmseqs2 enables sensitive protein sequence searching for the analysis of massive data sets. *Nature biotechnology*, 35(11):1026–1028, 2017.
- [46] P. Thölke and G. De Fabritiis. Torchmd-net: equivariant transformers for neural network based molecular potentials. *arXiv preprint arXiv:2202.02541*, 2022.
- [47] J. Tomasi and M. Persico. Molecular interactions in solution: an overview of methods based on continuous distributions of the solvent. *Chemical Reviews*, 94(7):2027–2094, 1994.
- [48] R. J. Townshend, M. Vögele, P. Suriana, A. Derry, A. Powers, Y. Laloudakis, S. Balachandar, B. Jing, B. Anderson, S. Eismann, et al. Atom3d: Tasks on molecules in three dimensions. *arXiv preprint arXiv:2012.04035*, 2020.
- [49] R. Tran, J. Lan, M. Shuaibi, B. M. Wood, S. Goyal, A. Das, J. Heras-Domingo, A. Kolluru, A. Rizvi, N. Shoghi, et al. The open catalyst 2022 (oc22) dataset and challenges for oxide electrocatalysts. *ACS Catalysis*, 13(5):3066–3084, 2023.
- [50] J. Vamathevan, D. Clark, P. Czodrowski, I. Dunham, E. Ferran, G. Lee, B. Li, A. Madabhushi, P. Shah, M. Spitzer, et al. Applications of machine learning in drug discovery and development. *Nature reviews Drug discovery*, 18(6):463–477, 2019.
- [51] A. Vaswani, N. Shazeer, N. Parmar, J. Uszkoreit, L. Jones, A. N. Gomez, Ł. Kaiser, and I. Polosukhin. Attention is all you need. *Advances in neural information processing systems*, 30, 2017.
- [52] T. Vreven, I. H. Moal, A. Vangone, B. G. Pierce, P. L. Kastiris, M. Torchala, R. Chaleil, B. Jiménez-García, P. A. Bates, J. Fernandez-Recio, et al. Updates to the integrated protein–protein interaction benchmarks: docking benchmark version 5 and affinity benchmark version 2. *Journal of molecular biology*, 427(19):3031–3041, 2015.
- [53] L. Wang, H. Liu, Y. Liu, J. Kurtin, and S. Ji. Learning protein representations via complete 3d graph networks. *arXiv preprint arXiv:2207.12600*, 2022.
- [54] R. Wang, X. Fang, Y. Lu, and S. Wang. The pdbind database: Collection of binding affinities for protein–ligand complexes with known three-dimensional structures. *Journal of medicinal chemistry*, 47(12):2977–2980, 2004.
- [55] J. D. Watson and F. H. Crick. The structure of dna. In *Cold Spring Harbor symposia on quantitative biology*, volume 18, pages 123–131. Cold Spring Harbor Laboratory Press, 1953.
- [56] M. Xu, L. Yu, Y. Song, C. Shi, S. Ermon, and J. Tang. Geodiff: A geometric diffusion model for molecular conformation generation. *arXiv preprint arXiv:2203.02923*, 2022.

- [57] S. Zaidi, M. Schaarschmidt, J. Martens, H. Kim, Y. W. Teh, A. Sanchez-Gonzalez, P. Battaglia, R. Pascanu, and J. Godwin. Pre-training via denoising for molecular property prediction. *arXiv preprint arXiv:2206.00133*, 2022.
- [58] Y. Zhang, H. Cai, C. Shi, B. Zhong, and J. Tang. E3bind: An end-to-end equivariant network for protein-ligand docking. *arXiv preprint arXiv:2210.06069*, 2022.
- [59] Z. Zhang, M. Xu, A. Jamasb, V. Chenthamarakshan, A. Lozano, P. Das, and J. Tang. Protein representation learning by geometric structure pretraining. *arXiv preprint arXiv:2203.06125*, 2022.

A Atom Position Code

Certain types of molecules have conventional position codes to distinguish different status of the atoms in the same block. For example, in the protein domain, where building blocks are residues, each atom in a residue is assigned a position code ($\alpha, \beta, \gamma, \delta, \epsilon, \zeta, \eta, \dots$) according to the number of chemical bonds between it and the alpha carbon (i.e. C_α). As these position codes provide meaningful heuristics of intra-block geometry, we also include them as a component of the embedding. For other types of molecules without such position codes (e.g. small molecules), we assign a [BLANK] type for positional embedding.

B Scheme of the Generalist Equivariant Transformer

We depict the overall workflow and the details of the equivariant bilevel attention module in Figure 4.

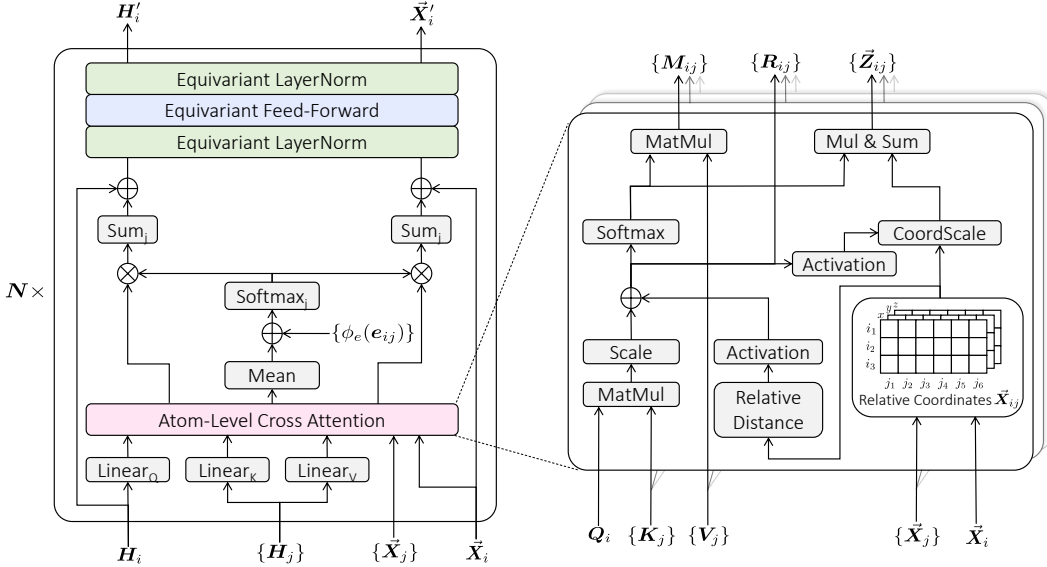


Figure 4: The scheme of a layer of Generalist Equivariant Transformer, where block i (H_i, \vec{X}_i) is updated by its neighbors ($\{H_j\}, \{\vec{X}_j\}, j \in \mathcal{N}_i(i)$). \otimes and \oplus denote multiplication and addition, respectively. (Left) The overall workflow of a layer and details of the block-level attention. (Right) The details of the atom-level cross attention. GET is composed of N such layers.

C Proof of E(3)-Equivariance and Intra-Block Permutation Invariance

Theorem C.1 (E(3)-Equivariance and Intra-Block Permutation Invariance). *Denote the proposed Equivariant Transformer as $\{H'_i, \vec{X}'_i\} = \text{GET}(\{H_i, \vec{X}_i\})$, then it conforms to E(3)-Equivariance and Intra-Block Permutation Invariance. Namely, $\forall g \in E(3), \forall \{\pi_i \in S_{n_i} | 1 \leq i \leq B\}$, where B is the number of blocks in the input and S_{n_i} includes all permutations on n_i elements, we have $\{\pi_i \cdot H'_i, \pi_i \cdot g \cdot \vec{X}'_i\} = \text{GET}(\{\pi_i \cdot H_i, \pi_i \cdot g \cdot \vec{X}_i\})$.*

The Generalist Equivariant Transformer (GET) is the cascading of the three types of modules: bilevel attention, feed-forward network, and layer normalization. Further, the E(3)-equivariance and the intra-block permutation invariance are disentangled. Therefore, the proof of its E(3)-equivariance and its invariance respect to the intra-block permutations can be decomposed into proof of these two properties on each module, which we present below.

C.1 Proof of E(3)-Equivariance

First we give the definition of E(3)-equivariance as follows:

Definition C.2 (E(3)-equivariance). A function $\phi : \mathbb{X} \rightarrow \mathbb{Y}$ conforms E(3)-equivariance if $\forall g \in E(3)$, the equation $\rho_{\mathbb{Y}}(g)\mathbf{y} = \phi(\rho_{\mathbb{X}}(g)\mathbf{x})$ holds true, where $\rho_{\mathbb{X}}$ and $\rho_{\mathbb{Y}}$ instantiate g in \mathbb{X} and \mathbb{Y} , respectively. A special case is E(3)-invariance where $\rho_{\mathbb{Y}}$ constantly outputs identity transformation (i.e. $\rho_{\mathbb{Y}}(g) \equiv I$).

Given $g \in E(3)$ and $\vec{x} \in \mathbb{R}^3$, we can instantiate g as $g \cdot \vec{x} := \mathbf{Q}\vec{x} + \vec{t}$, where $\mathbf{Q} \in \mathbb{R}^{3 \times 3}$ is an orthogonal matrix and $\vec{t} \in \mathbb{R}^3$ is a translation vector. Implementing g on a coordinate matrix $\vec{X} \in \mathbb{R}^{n \times 3}$ means transforming each coordinate (i.e. each row) with g .

Then we prove the E(3)-equivariance of each module in GET as follows:

Lemma C.3. Denote the bilevel attention module as $\{\mathbf{H}'_i, \vec{X}'_i\} = \text{Att}(\{\mathbf{H}_i, \vec{X}_i\})$, then it is E(3)-equivariant. Namely, $\forall g \in E(3)$, we have $\{\mathbf{H}'_i, g \cdot \vec{X}'_i\} = \text{Att}(\{\mathbf{H}_i, g \cdot \vec{X}_i\})$.

Proof. The key to the proof of Lemma C.3 is to prove that the propagation in Eq. 2-8 is E(3)-invariant on \mathbf{H}_i and E(3)-equivariant on \vec{X}_i . Obviously, the correlation \mathbf{R}_{ij} between block i and block j in Eq. 3 is E(3)-invariant because all the inputs, that is, the query, the key, and the distance matrices, are not affected by the geometric transformation g . Therefore, we can immediately derive that the atom-level cross attention α_{ij} in Eq. 4 is E(3)-invariant. Similarly, the block-level attention β_{ij} in Eq. 6 is E(3)-invariant because it only operates on r_{ij} in Eq. 5 which aggregates α_{ij} and the edge feature. Finally, we can derive the E(3)-invariance on \mathbf{H} and the E(3)-equivariance on \vec{X} :

$$\begin{aligned}
\mathbf{H}'_i[p] &= \mathbf{H}_i[p] + \sum_{j \in \mathcal{N}(i)} \beta_{ij} \phi_m(\alpha_{ij}[p] \cdot \mathbf{V}_j), \\
g \cdot \vec{X}'_i[p] &= g \cdot (\vec{X}_i[p] + \sum_{j \in \mathcal{N}(i)} \beta_{ij} (\alpha_{ij}[p] \odot \phi_X(\mathbf{R}_{ij}[p])) \cdot \vec{X}_{ij}[p]) \\
&= \mathbf{Q}(\vec{X}_i[p] + \sum_{j \in \mathcal{N}(i)} \beta_{ij} (\alpha_{ij}[p] \odot \phi_X(\mathbf{R}_{ij}[p])) \cdot \vec{X}_{ij}[p]) + \vec{t} \\
&= (\mathbf{Q}\vec{X}_i[p] + \vec{t}) + \sum_{j \in \mathcal{N}(i)} \beta_{ij} (\alpha_{ij}[p] \odot \phi_X(\mathbf{R}_{ij}[p])) \cdot \begin{bmatrix} \mathbf{Q}(\vec{X}_i[p] - \vec{X}_j[1]) \\ \vdots \\ \mathbf{Q}(\vec{X}_i[p] - \vec{X}_j[n_j]) \end{bmatrix} \\
&= (\mathbf{Q}\vec{X}_i[p] + \vec{t}) + \sum_{j \in \mathcal{N}(i)} \beta_{ij} (\alpha_{ij}[p] \odot \phi_X(\mathbf{R}_{ij}[p])) \cdot \begin{bmatrix} \mathbf{Q}\vec{X}_i[p] + \vec{t} - (\mathbf{Q}\vec{X}_j[1] + \vec{t}) \\ \vdots \\ \mathbf{Q}\vec{X}_i[p] + \vec{t} - (\mathbf{Q}\vec{X}_j[n_j] + \vec{t}) \end{bmatrix} \\
&= g \cdot \vec{X}_i[p] + \sum_{j \in \mathcal{N}(i)} \beta_{ij} (\alpha_{ij}[p] \odot \phi_X(\mathbf{R}_{ij}[p])) \cdot \begin{bmatrix} g \cdot \vec{X}_i[p] - g \cdot \vec{X}_j[1] \\ \vdots \\ g \cdot \vec{X}_i[p] - g \cdot \vec{X}_j[n_j] \end{bmatrix},
\end{aligned}$$

which concludes the proof of Lemma C.3. \square

Lemma C.4. Denote the equivariant feed-forward network as $\{\mathbf{H}'_i, \vec{X}'_i\} = \text{FFN}(\{\mathbf{H}_i, \vec{X}_i\})$, then it is E(3)-equivariant. Namely, $\forall g \in E(3)$, we have $\{\mathbf{H}'_i, g \cdot \vec{X}'_i\} = \text{FFN}(\{\mathbf{H}_i, g \cdot \vec{X}_i\})$.

Proof. The proof of Lemma C.4 focuses on the single-atom updates in Eq. 9-12. First, it is easy to obtain the E(3)-equivariance of the centroid in Eq. 9:

$$g \cdot \vec{x}_c = g \cdot \text{centroid}(\vec{X}_i) = \text{centroid}(g \cdot \vec{X}_i).$$

Then we have the following equation on the relative coordinate $\Delta\vec{x}$ in Eq. 10:

$$\mathbf{Q}\Delta\vec{x} = (\mathbf{Q}\vec{x} + \vec{t}) - (\mathbf{Q}\vec{x}_c + \vec{t}) = g \cdot \vec{x} - g \cdot \vec{x}_c.$$

We can immediately obtain the E(3)-invariance of r in Eq. 10:

$$r = \phi_r\left(\frac{(\mathbf{Q}\Delta\vec{x})^\top (\mathbf{Q}\Delta\vec{x})}{C + \|(\mathbf{Q}\Delta\vec{x})^\top (\mathbf{Q}\Delta\vec{x})\|}\right) = \phi_r\left(\frac{\Delta\vec{x}^\top \mathbf{Q}^\top \mathbf{Q} \Delta\vec{x}}{C + \|\Delta\vec{x}^\top \mathbf{Q}^\top \mathbf{Q} \Delta\vec{x}\|}\right) = \phi_r\left(\frac{\Delta\vec{x}^\top \Delta\vec{x}}{C + \|\Delta\vec{x}^\top \Delta\vec{x}\|}\right).$$

Finally we can derive the E(3)-invariance on \mathbf{h} and the E(3)-equivariance on $\vec{\mathbf{x}}$:

$$\begin{aligned}
\mathbf{h}' &= \mathbf{h} + \phi_h(\mathbf{h}, \mathbf{h}_c, \mathbf{r}), \\
g \cdot \vec{\mathbf{x}}' &= g \cdot (\vec{\mathbf{x}} + \Delta \vec{\mathbf{x}} \phi_x(\mathbf{h}, \mathbf{h}_c, \mathbf{r})) \\
&= \mathbf{Q}(\vec{\mathbf{x}} + \Delta \vec{\mathbf{x}} \phi_x(\mathbf{h}, \mathbf{h}_c, \mathbf{r})) + \vec{\mathbf{t}} \\
&= \mathbf{Q}\vec{\mathbf{x}} + \vec{\mathbf{t}} + \mathbf{Q}\Delta \vec{\mathbf{x}} \phi_x(\mathbf{h}, \mathbf{h}_c, \mathbf{r}) \\
&= g \cdot \vec{\mathbf{x}} + (g \cdot \vec{\mathbf{x}} - g \cdot \vec{\mathbf{x}}_c) \phi_x(\mathbf{h}, \mathbf{h}_c, \mathbf{r}) \\
&= g \cdot \vec{\mathbf{x}} + (g \cdot \vec{\mathbf{x}} - \text{centroid}(g \cdot \vec{\mathbf{X}}_i)) \phi_x(\mathbf{h}, \mathbf{h}_c, \mathbf{r}),
\end{aligned}$$

which concludes the proof of Lemma C.4 \square

Lemma C.5. Denote the equivariant layer normalization as $\{\mathbf{H}'_i, \vec{\mathbf{X}}'_i\} = \text{ELN}(\{\mathbf{H}_i, \vec{\mathbf{X}}_i\})$, then it is E(3)-equivariant. Namely, $\forall g \in E(3)$, we have $\{\mathbf{H}'_i, g \cdot \vec{\mathbf{X}}'_i\} = \text{ELN}(\{\mathbf{H}_i, g \cdot \vec{\mathbf{X}}_i\})$.

Proof. Since the layer normalization is implemented on the atom level, namely each row of the coordinate matrix in a node, we again only need to concentrate on the single-atom normalization in Eq. 13-14. The key points lie in the E(3)-equivariance of $\mathbb{E}[\vec{\mathbf{X}}]$ and the E(3)-invariance of $\text{Var}[\vec{\mathbf{X}} - \mathbb{E}[\vec{\mathbf{X}}]]$. The first one is obvious because $\mathbb{E}[\vec{\mathbf{X}}]$ is the centroid of the coordinates of all atoms:

$$g \cdot \mathbb{E}[\vec{\mathbf{X}}] = g \cdot \text{centroid}(\vec{\mathbf{X}}) = \text{centroid}(g \cdot \vec{\mathbf{X}}) = \mathbb{E}[g \cdot \vec{\mathbf{X}}].$$

Suppose there are N atoms in total, then we can prove the E(3)-invariance of the variance as follows:

$$\begin{aligned}
\text{Var}[\vec{\mathbf{X}} - \mathbb{E}[\vec{\mathbf{X}}]] &= \frac{\sum_{i=1}^N (x_i - \bar{x})^2 + \sum_{i=1}^N (y_i - \bar{y})^2 + \sum_{i=1}^N (z_i - \bar{z})^2}{3N} \\
&= \frac{\sum_{i=1}^N [(x_i - \bar{x})^2 + (y_i - \bar{y})^2 + (z_i - \bar{z})^2]}{3N} \\
&= \frac{\sum_{i=1}^N (\vec{\mathbf{x}}_i - \mathbb{E}[\vec{\mathbf{X}}])^\top (\vec{\mathbf{x}}_i - \mathbb{E}[\vec{\mathbf{X}}])}{3N} \\
&= \frac{\sum_{i=1}^N (\vec{\mathbf{x}}_i - \mathbb{E}[\vec{\mathbf{X}}])^\top \mathbf{Q}^\top \mathbf{Q} (\vec{\mathbf{x}}_i - \mathbb{E}[\vec{\mathbf{X}}])}{3N} \\
&= \frac{\sum_{i=1}^N (\mathbf{Q}\vec{\mathbf{x}}_i - \mathbf{Q}\mathbb{E}[\vec{\mathbf{X}}])^\top (\mathbf{Q}\vec{\mathbf{x}}_i - \mathbf{Q}\mathbb{E}[\vec{\mathbf{X}}])}{3N} \\
&= \frac{\sum_{i=1}^N (g \cdot \vec{\mathbf{x}}_i - g \cdot \mathbb{E}[\vec{\mathbf{X}}])^\top (g \cdot \vec{\mathbf{x}}_i - g \cdot \mathbb{E}[\vec{\mathbf{X}}])}{3N} \\
&= \frac{\sum_{i=1}^N (g \cdot \vec{\mathbf{x}}_i - \mathbb{E}[g \cdot \vec{\mathbf{X}}])^\top (g \cdot \vec{\mathbf{x}}_i - \mathbb{E}[g \cdot \vec{\mathbf{X}}])}{3N} \\
&= \text{Var}[g \cdot \vec{\mathbf{X}} - \mathbb{E}[g \cdot \vec{\mathbf{X}}]].
\end{aligned}$$

Therefore, we can finally derive the E(3)-invariance on \mathbf{h} and the E(3)-equivariance on $\vec{\mathbf{x}}$ in Eq. 13-14:

$$\begin{aligned}
\mathbf{h} &= \frac{\mathbf{h} - \mathbb{E}[\mathbf{h}]}{\sqrt{\text{Var}[\mathbf{h}]}} \cdot \gamma + \beta, \\
g \cdot \vec{\mathbf{x}} &= g \cdot \left(\frac{\vec{\mathbf{x}} - \mathbb{E}[\vec{\mathbf{X}}]}{\sqrt{\text{Var}[\vec{\mathbf{X}} - \mathbb{E}[\vec{\mathbf{X}}]]}} \cdot \sigma + \mathbb{E}[\vec{\mathbf{X}}] \right) = \frac{\mathbf{Q}\vec{\mathbf{x}} - \mathbf{Q}\mathbb{E}[\vec{\mathbf{X}}]}{\sqrt{\text{Var}[\vec{\mathbf{X}} - \mathbb{E}[\vec{\mathbf{X}}]]}} \cdot \sigma + \mathbf{Q}\mathbb{E}[\vec{\mathbf{X}}] + \vec{\mathbf{t}} \\
&= \frac{\mathbf{Q}\vec{\mathbf{x}} + \vec{\mathbf{t}} - (\mathbf{Q}\mathbb{E}[\vec{\mathbf{X}}] + \vec{\mathbf{t}})}{\sqrt{\text{Var}[\vec{\mathbf{X}} - \mathbb{E}[\vec{\mathbf{X}}]]}} \cdot \sigma + (\mathbf{Q}\mathbb{E}[\vec{\mathbf{X}}] + \vec{\mathbf{t}}) = \frac{g \cdot \vec{\mathbf{x}} - g \cdot \mathbb{E}[\vec{\mathbf{X}}]}{\sqrt{\text{Var}[g \cdot \vec{\mathbf{X}} - \mathbb{E}[g \cdot \vec{\mathbf{X}}]]}} \cdot \sigma + g \cdot \mathbb{E}[\vec{\mathbf{X}}] \\
&= \frac{g \cdot \vec{\mathbf{x}} - \mathbb{E}[g \cdot \vec{\mathbf{X}}]}{\sqrt{\text{Var}[g \cdot \vec{\mathbf{X}} - \mathbb{E}[g \cdot \vec{\mathbf{X}}]]}} \cdot \sigma + \mathbb{E}[g \cdot \vec{\mathbf{X}}],
\end{aligned}$$

which concludes the proof of Lemma C.5. \square

With Lemma C.3-C.5 at hand, it is obvious to deduce the E(3)-equivariance of the GET layer.

C.2 Proof of Intra-Block Permutation Invariance

Obviously, the feed-forward network and the layer normalization are invariant to intra-block permutations because they are implemented on single atoms and the only incorporated multi-atom operation is averaging, which is invariant to the permutations. Therefore, the proof narrows down to the intra-block permutation invariance of the bilevel attention module.

Lemma C.6. *Denote the bilevel attention module as $\{\mathbf{H}'_i, \vec{\mathbf{X}}'_i\} = \text{Att}(\{\mathbf{H}_i, \vec{\mathbf{X}}_i\})$, then it conforms to intra-block permutation invariance. Namely, $\forall \{\pi_i \in S_{n_i} | 1 \leq i \leq B\}$, where B is the number of blocks in the input and S_{n_i} includes all permutations on n_i elements, we have $\{\pi_i \cdot \mathbf{H}'_i, \pi_i \cdot \vec{\mathbf{X}}'_i\} = \text{Att}(\{\pi_i \cdot \mathbf{H}_i, \pi_i \cdot \vec{\mathbf{X}}_i\})$.*

Proof. Denote the the permutation of block i as π_i , then it can be instantiated as the multiplication of a series of elementary row-switching matrices $\mathbf{P}_i = \mathbf{P}_i^{(m_i)} \mathbf{P}_i^{(m_i-1)} \dots \mathbf{P}_i^{(1)}$. For example, we have $\pi_i \cdot \mathbf{H}_i = \mathbf{P}_i \mathbf{H}_i$, $\pi_i \cdot \vec{\mathbf{X}}_i = \mathbf{P}_i \vec{\mathbf{X}}_i$. Here we first prove an elegant property of \mathbf{P}_i , which we will use in the later proof:

$$\begin{aligned} \mathbf{P}_i^\top \mathbf{P}_i &= (\mathbf{P}_i^{(m_i)} \mathbf{P}_i^{(m_i-1)} \dots \mathbf{P}_i^{(1)})^\top (\mathbf{P}_i^{(m_i)} \mathbf{P}_i^{(m_i-1)} \dots \mathbf{P}_i^{(1)}) \\ &= \mathbf{P}_i^{(1)\top} \dots \mathbf{P}_i^{(m_i-1)\top} \mathbf{P}_i^{(m_i)\top} \mathbf{P}_i^{(m_i)} \mathbf{P}_i^{(m_i-1)} \dots \mathbf{P}_i^{(1)} \\ &= \mathbf{P}_i^{(1)\top} \dots \mathbf{P}_i^{(m_i-1)\top} \mathbf{I} \mathbf{P}_i^{(m_i-1)} \dots \mathbf{P}_i^{(1)} \\ &= \dots \\ &= \mathbf{I} \end{aligned}$$

Given arbitrary permutations on each block, we have the permuted query, key, and value matrices:

$$\begin{aligned} \mathbf{P}_i \mathbf{Q}_i &= \mathbf{P}_i \mathbf{H}_i \mathbf{W}_Q = (\pi_i \cdot \mathbf{H}_i) \mathbf{W}_Q, \\ \mathbf{P}_i \mathbf{K}_i &= \mathbf{P}_i \mathbf{H}_i \mathbf{W}_K = (\pi_i \cdot \mathbf{H}_i) \mathbf{W}_K, \\ \mathbf{P}_i \mathbf{V}_i &= \mathbf{P}_i \mathbf{H}_i \mathbf{W}_V = (\pi_i \cdot \mathbf{H}_i) \mathbf{W}_V. \end{aligned}$$

The distance matrix \mathbf{D}_{ij} is also permuted as $\mathbf{P}_i \mathbf{D}_{ij} \mathbf{P}_j^\top$. Therefore, the atom-level attention α_{ij} in Eq. 4 is also permuted as:

$$\begin{aligned} \mathbf{P}_i \mathbf{R}_{ij} \mathbf{P}_j^\top &= \frac{1}{\sqrt{d_r}} (\mathbf{P}_i \mathbf{Q}_i (\mathbf{P}_j \mathbf{K}_j)^\top) + \sigma_D (\mathbf{P}_i \mathbf{D}_{ij} \mathbf{P}_j^\top) = \mathbf{P}_i \left(\frac{1}{\sqrt{d_r}} (\mathbf{Q}_i \mathbf{K}_j^\top) + \sigma_D (\mathbf{D}_{ij}) \right) \mathbf{P}_j^\top, \\ \mathbf{P}_i \alpha_{ij} \mathbf{P}_j^\top &= \text{Softmax}(\mathbf{P}_i \mathbf{R}_{ij} \mathbf{P}_j^\top) = \mathbf{P}_i \text{Softmax}(\mathbf{R}_{ij}) \mathbf{P}_j^\top. \end{aligned}$$

The block-level attention β_{ij} in Eq. 6 remains unchanged as the average of \mathbf{R}_{ij} in obtaining r_{ij} eliminates the effect of permutations. Finally, we can derive the intra-block permutation invariance as follows:

$$\begin{aligned} \mathbf{P}_i \mathbf{H}'_i &= \mathbf{P}_i \begin{bmatrix} \mathbf{H}'_i[1] \\ \vdots \\ \mathbf{H}'_i[n_i] \end{bmatrix} = \mathbf{P}_i \begin{bmatrix} \mathbf{H}_i[1] + \sum_{j \in \mathcal{N}(i)} \beta_{ij} \phi_m(\alpha_{ij}[1] \mathbf{P}_j^\top \mathbf{P}_j \mathbf{V}_j) \\ \vdots \\ \mathbf{H}_i[n_i] + \sum_{j \in \mathcal{N}(i)} \beta_{ij} \phi_m(\alpha_{ij}[n_i] \mathbf{P}_j^\top \mathbf{P}_j \mathbf{V}_j) \end{bmatrix} \\ &= \mathbf{P}_i \begin{bmatrix} \mathbf{H}_i[1] + \sum_{j \in \mathcal{N}(i)} \beta_{ij} \phi_m(\alpha_{ij}[1] \mathbf{V}_j) \\ \vdots \\ \mathbf{H}_i[n_i] + \sum_{j \in \mathcal{N}(i)} \beta_{ij} \phi_m(\alpha_{ij}[n_i] \mathbf{V}_j) \end{bmatrix} \\ \mathbf{P}_i \vec{\mathbf{X}}'_i &= \mathbf{P}_i \begin{bmatrix} \vec{\mathbf{X}}'_i[1] \\ \vdots \\ \vec{\mathbf{X}}'_i[n_i] \end{bmatrix} = \mathbf{P}_i \begin{bmatrix} \vec{\mathbf{X}}_i[1] + \sum_{j \in \mathcal{N}(i)} \beta_{ij} (\alpha_{ij}[1] \odot \phi_X(\mathbf{R}_{ij}[1])) \mathbf{P}_j^\top \mathbf{P}_j \vec{\mathbf{X}}_{ij}[1] \\ \vdots \\ \vec{\mathbf{X}}_i[n_i] + \sum_{j \in \mathcal{N}(i)} \beta_{ij} (\alpha_{ij}[n_i] \odot \phi_X(\mathbf{R}_{ij}[n_i])) \mathbf{P}_j^\top \mathbf{P}_j \vec{\mathbf{X}}_{ij}[n_i] \end{bmatrix} \\ &= \mathbf{P}_i \begin{bmatrix} \vec{\mathbf{X}}_i[1] + \sum_{j \in \mathcal{N}(i)} \beta_{ij} (\alpha_{ij}[1] \odot \phi_X(\mathbf{R}_{ij}[1])) \vec{\mathbf{X}}_{ij}[1] \\ \vdots \\ \vec{\mathbf{X}}_i[n_i] + \sum_{j \in \mathcal{N}(i)} \beta_{ij} (\alpha_{ij}[n_i] \odot \phi_X(\mathbf{R}_{ij}[n_i])) \vec{\mathbf{X}}_{ij}[n_i] \end{bmatrix}, \end{aligned}$$

which concludes Lemma C.6. \square

D Implementation Details

We conduct experiments on 1 GeForce RTX 2080 Ti GPU. Each model is trained with Adam optimizer and exponential learning rate decay. To avoid unstable checkpoints from early training stages, we select the latest checkpoint from the saved top- k checkpoints on the validation set for testing. Since the number of blocks varies a lot in different samples, we set a upperbound of the number of blocks to form a dynamic batch instead of using a static batch size. We use $k = 9$ for constructing the k-nearest neighbor graph in § 3.1. We give the description of the hyperparameters in Table 4 and their values for each task in Table 5.

Table 4: Descriptions of the hyperparameters.

hyperparameter	description
d_h	Hidden size
d_r	Hidden size
lr	Learning rate
final_lr	Final learning rate
max_epoch	Maximum of epochs to train
save_topk	Number of top- k checkpoints to save
n_layers	Number of layers
max_n_vertex	Upperbound of the number of nodes in a batch

Table 5: Hyperparameters for our GET on each task.

hyperparameter	PPA	LBA	LEP	hyperparameter	PPA	LBA	LEP
GET							
d_h	128	64	64	d_r	16	32	64
lr	10^{-4}	10^{-3}	10^{-3}	final_lr	10^{-4}	10^{-6}	10^{-4}
max_epoch	20	10	65	save_topk	3	3	5
n_layers	3	3	3	max_n_vertex	1500	2000	1500
GET-mix							
d_h	128	128	-	d_r	16	16	-
lr	5×10^{-5}	5×10^{-5}	-	final_lr	5×10^{-5}	10^{-6}	-
max_epoch	20	20	-	save_topk	3	3	-
n_layers	3	3	-	max_n_vertex	1500	1500	-

E Baselines

In this section, we describe the implementation details of different baselines. All the baselines are designed for structural learning on graphs whose nodes are represented as one feature vector and one coordinate. Therefore, for **block-level** representation, we average the embeddings and the coordinates of the atoms in each block before feeding the graph to the baselines. For **atom-level** representation, each node is represented as the embedding and the coordinate of each atom. For fair comparison, the number of layers in each model is set to 3. We present other hyperparameters in Table 6.

SchNet [41] We use the implementation in PyTorch Geometric and project the edge feature into the same shape as the distance feature expanded with radial basis functions. Then we add the edge feature to the expanded distance feature as the edge attribute for fair comparison across different models.

DimeNet++ [11, 10] We use the implementation in PyTorch Geometric. Since the spherical basis functions used in DimeNet++ model the angles between any two neighbors of each node, the complexity is much higher than other baselines. Therefore, we fail to run atom-level DimeNet++ in

the PPA task due to the large number of nodes in atom-level decomposition of proteins. Also, the atom-level DimeNet++ in the PLA task need 2 GeForce RTX 2080 Ti GPU for training.

EGNN [40] We directly use the official open-source codes provided in the original paper of EGNN.

TorchMD-Net [46] We directly use the official implementation in the original paper. Similar to the adaption of SchNet, we also add the edge feature to the expanded distance for fair comparison.

Table 6: Hyperparameters for each baseline on each task.

hyperparameter	PPA	LBA	LEP	hyperparameter	PPA	LBA	LEP
SchNet							
d_h	128	64	64	max_n_vertex	1500	1500	1500
lr	10^{-3}	5×10^{-4}	10^{-3}	final_lr	10^{-4}	10^{-5}	10^{-4}
max_epoch	20	60	65	save_topk	3	5	5
SchNet-mix							
d_h	128	128	-	max_n_vertex	1500	1500	-
lr	5×10^{-5}	5×10^{-5}	-	final_lr	5×10^{-5}	5×10^{-5}	-
max_epoch	20	20	-	save_topk	3	3	-
DimeNet++							
d_h	128	64	64	max_n_vertex	1500	1500	1500
lr	10^{-3}	5×10^{-4}	10^{-3}	final_lr	10^{-4}	10^{-5}	10^{-4}
max_epoch	20	60	65	save_topk	3	5	5
EGNN							
d_h	128	64	64	max_n_vertex	1500	1500	1500
lr	10^{-3}	5×10^{-4}	10^{-3}	final_lr	10^{-4}	10^{-5}	10^{-4}
max_epoch	20	60	65	save_topk	3	5	5
TorchMD-Net							
d_h	128	64	64	max_n_vertex	1500 ³	1500	1500
lr	10^{-3}	5×10^{-4}	10^{-3}	final_lr	10^{-4}	10^{-5}	10^{-4}
max_epoch	20	20	65	save_topk	3	3	5
TorchMD-Net-mix							
d_h	128	128	-	max_n_vertex	1500	1500	-
lr	5×10^{-5}	5×10^{-5}	-	final_lr	5×10^{-5}	5×10^{-5}	-
max_epoch	20	20	-	save_topk	3	3	-

F Detailed Results of Universal Learning of Molecular Interaction Affinity

We provide the mean and the standard deviation of three parallel experiments on the universal learning of molecular interaction affinity (§ 4.4) in Tables 7 and 8.

³The value for the atom-level model is set to be 750 due to the higher complexity.

Table 7: The mean and the standard deviation of three runs on protein-protein affinity prediction. Methods with the suffix "-mix" are trained on the mixed dataset of protein-protein affinity and ligand binding affinity. The best results are marked in bold and the second best are underlined.

Repr.	Model	Rigid	Medium	Flexible	All
Pearson \uparrow					
Block	SchNet	0.542 \pm 0.012	0.504 \pm 0.020	0.102 \pm 0.019	0.439 \pm 0.016
	SchNet-mix	0.553 \pm 0.029	0.507 \pm 0.011	0.093 \pm 0.041	0.434 \pm 0.011
	TorchMD-Net	0.575 \pm 0.041	0.470 \pm 0.024	0.087 \pm 0.024	0.424 \pm 0.021
	TorchMD-Net-mix	0.579 \pm 0.028	0.502 \pm 0.019	0.179 \pm 0.044	0.457 \pm 0.011
Atom	SchNet	0.592 \pm 0.007	0.522 \pm 0.010	-0.038 \pm 0.016	0.369 \pm 0.007
	SchNet-mix	<u>0.625 \pm 0.017</u>	0.520 \pm 0.021	-0.012 \pm 0.049	0.421 \pm 0.019
	TorchMD-Net	0.609 \pm 0.023	0.486 \pm 0.004	0.049 \pm 0.009	0.401 \pm 0.005
	TorchMD-Net-mix	0.618 \pm 0.048	0.444 \pm 0.027	0.057 \pm 0.125	0.382 \pm 0.029
Unified	GET (ours)	0.604 \pm 0.016	<u>0.524 \pm 0.013</u>	<u>0.301 \pm 0.056</u>	<u>0.481 \pm 0.008</u>
	GET-mix (ours)	0.640 \pm 0.060	0.533 \pm 0.022	0.354 \pm 0.029	0.491 \pm 0.015
Spearman \uparrow					
Block	SchNet	0.476 \pm 0.015	0.520 \pm 0.013	0.068 \pm 0.009	0.427 \pm 0.012
	SchNet-mix	0.497 \pm 0.044	<u>0.527 \pm 0.009</u>	0.042 \pm 0.031	0.426 \pm 0.007
	TorchMD-Net	0.552 \pm 0.039	0.482 \pm 0.025	0.090 \pm 0.062	0.415 \pm 0.027
	TorchMD-Net-mix	0.550 \pm 0.039	0.524 \pm 0.019	0.188 \pm 0.070	0.472 \pm 0.019
Atom	SchNet	0.546 \pm 0.005	0.512 \pm 0.007	0.028 \pm 0.032	0.404 \pm 0.016
	SchNet-mix	0.557 \pm 0.042	0.516 \pm 0.033	0.036 \pm 0.010	0.428 \pm 0.022
	TorchMD-Net	0.582 \pm 0.025	0.487 \pm 0.002	0.117 \pm 0.008	0.436 \pm 0.004
	TorchMD-Net-mix	<u>0.608 \pm 0.040</u>	0.453 \pm 0.037	0.058 \pm 0.135	0.394 \pm 0.027
Unified	GET (ours)	0.580 \pm 0.011	<u>0.527 \pm 0.005</u>	<u>0.300 \pm 0.056</u>	<u>0.495 \pm 0.011</u>
	GET-mix (ours)	0.614 \pm 0.024	0.546 \pm 0.019	0.355 \pm 0.014	0.511 \pm 0.016

Table 8: The mean and the standard deviation of three runs on ligand binding affinity prediction. Methods with the suffix "-mix" are trained on the mixed dataset of protein-protein affinity and ligand binding affinity. The best results are marked in bold and the second best are underlined.

Repr.	Model	LBA		
		RMSE \downarrow	Pearson \uparrow	Spearman \uparrow
Block	SchNet	1.406 \pm 0.020	0.565 \pm 0.006	0.549 \pm 0.007
	SchNet-mix	1.385 \pm 0.016	0.573 \pm 0.011	0.553 \pm 0.012
	TorchMD-net	1.367 \pm 0.037	0.599 \pm 0.017	0.584 \pm 0.025
	TorchMD-net-mix	1.423 \pm 0.054	0.586 \pm 0.012	0.567 \pm 0.019
Atom	SchNet	1.357 \pm 0.017	0.598 \pm 0.011	0.592 \pm 0.015
	SchNet-mix	<u>1.365 \pm 0.010</u>	0.589 \pm 0.006	0.575 \pm 0.009
	TorchMD-net	1.381 \pm 0.013	0.591 \pm 0.007	0.583 \pm 0.009
	TorchMD-net-mix	1.448 \pm 0.122	0.566 \pm 0.061	0.564 \pm 0.059
Unified	GET (ours)	1.446 \pm 0.012	<u>0.600 \pm 0.002</u>	<u>0.606 \pm 0.002</u>
	GET-mix (ours)	1.370 \pm 0.008	0.606 \pm 0.003	0.606 \pm 0.003